Nano World Journal

https://doi.org/10.17756/nwj.2023-s2-031

Research Article

Open Access

Effect of Fly Ash on the Sustainability of Water Treatment Reservoir Concrete Subjected to 3.5% $Al_2(SO_4)_3$ by Electrochemical Impedance Spectroscopy

Adil Ech-chebab[1*], Aadil Ejbouh[1], Mouhsine Galai[1], Redouane Lachhab[1], Tounsi Belhaj[2] and Mohamed Ebn Touhami[1]

[1]*Laboratory of Advanced Materials and Process Engineering, Faculty of Sciences, University Ibn Tofail, PB. 133, Kenitra, Morocco*

[2]*International Institute for Water and Sanitation (IEA), National Office of Electricity and Drinking Water (ONEE), Rabat, Morocco*

***Correspondence to:**
Adil Ech-chebab
Laboratory of Advanced Materials and Process Engineering,
Faculty of Sciences, University Ibn Tofail, PB. 133, Kenitra, Morocco
E-mail: adilechchebab@gmail.com

Received: July 25, 2023
Accepted: September 25, 2023
Published: September 28, 2023

Citation: Ech-chebab A, Ejbouh A, Galai M, Lachhab R, Belhaj T, et al. 2023. Effect of Fly Ash on the Sustainability of Water Treatment Reservoir Concrete Subjected to 3.5% $Al_2(SO_4)_3$ by Electrochemical Impedance Spectroscopy. *NanoWorld J* 9(S2): S174-S179.

Copyright: © 2023 Ech-chebab et al. This is an Open Access article distributed under the terms of the Creative Commons Attribution 4.0 International License (CCBY) (http://creativecommons.org/licenses/by/4.0/) which permits commercial use, including reproduction, adaptation, and distribution of the article provided the original author and source are credited.

Published by United Scientific Group

Abstract

This paper presents an experimental study aimed at improving the durability of reinforced concrete water treatment reservoirs exposed to a high concentration of the water treatment coagulant $Al_2(SO_4)_3$. This investigation was carried out using electrochemical methods. The sulfate concentration of 3.5% was chosen to meet the requirements of exposure class XA3 according to standard NF EN 206-1. The results were obtained from three concrete mixes: a control mix containing 100% ordinary Portland cement (OPC), and 25% fly ash (FA). The samples were immersed in the solution and then subjected to cyclic corrosion acceleration by means of an imposed voltage of 15 V. Electrochemical impedance spectroscopy (EIS) was used to monitor changes in the resistance of these concretes under accelerated corrosion. In addition, X-ray diffraction (XRD) was used to examine the corrosion products at the end of the tests. The results indicate that the mineral additives made substantial improvements to the durability of the concrete. Moreover, 25% FA gave the best results against corrosion.

Keywords

Durability, Concrete, Fly ash, Aluminum sulfate coagulant, Electrochemical impedance spectroscopy, X-ray diffraction

Introduction

Some water treatment stations use ($Al_2(SO_4)_3$) as a coagulant for water treatment. This chemical product is generally added during the initial phase of the coagulation process, to improve the removal of suspended solids, including colloidal particles, as well as natural organic matter [1]. Unfortunately, this coagulant contains sulfate ions, which are among the most common agents of deterioration in reinforced concrete constructions [2, 3]. These sulfate ions contribute to gypsum and ettringite crystal formation, which could result in expansion, loss of strength, cracking, and ultimately failure of the concrete structure [2-4]. The following reactions explain the mechanisms of formation of the expansive products in the case where the associated cation is the Na^+ ions (Eq 1 and 2) [5]:

$$Ca(OH)_2 + Na_2SO_4 + 2H_2O \rightarrow CaSO_4.2H_2O + 2NaOH \quad (1)$$

$$C_3A + 3CaSO_4.H_2O + 24\text{-}26H_2O \rightarrow C_3A.3CaSO_4.30\text{-}32H_2O \quad (2)$$

In the case where the associated cation is the Mg^{2+} ion (Eq 3, 4, and 5) [6]:

$$Ca(OH)_2 + MgSO_4 + 2H_2O \rightarrow CaSO_4.2H_2O + Mg(OH)_2 \quad (3)$$

$$C_3A + 3CaSO_4.H_2O + 26H_2O \rightarrow C_3A.3CaSO_4.32H_2O \quad (4)$$

$$C\text{-}S\text{-}H + MgSO_4 + 2H_2O \rightarrow CaSO_4.2H_2O + 5(C,M)\text{-}S\text{-}H \quad (5)$$

On the other hand, most of the studies were carried out under the effect of Na_2SO_4 or $MgSO_4$ attacks. But the study in the medium containing aluminum sulfate is rare [7].

The National Office of Electricity and potable Water (ONEE) in Morocco uses $Al_2(SO_4)_3$ as a coagulant in water treatment stations. But unfortunately, it is suffering from the attacks of this chemical. The attacks are more associated with the use of this coagulant at high concentrations. These kinds of failures threaten the integrity of the whole construction over time, leading to the rapid development of corrosion of the steel and concrete cladding [8]. After a thorough examination of these sites, it was revealed that the reparation was inadequate and did not stop the progress of the damage from inside the reservoir.

The replacement of cement with FA used in the construction of concrete structures is also a practical and environmentally friendly way [9] because of the reduction in the cost of construction and improvement of concrete durability in aggressive environments [10] such as sulfate [11, 12].

The pozzolanic effect produces a secondary gel that fills the capillary of concrete, improving its strength [13]. Sharma et al. [14] studied the compressive strength of M30 grade concrete specimens made by replacing 5, 10, and 15 percent of the cement with FA. The results of the study showed that the use of FA in concrete manufacturing as a partial replacement for cement can result in the development of more durable and stronger concrete. Huseien et al. [15] studied the durability performance of concrete incorporating FA. They found that the incorporation of FA in the concrete matrix improves the mechanical and durability characteristics of the modified concrete. In general, three primary strategies are recommended to compact sulfate attack including (1) limiting the C_3A content in cement as prescribed in ASTMC150, (2) reducing the calcium hydroxides content by using supplementary cementitious material as a cement replacing material, and (3) reducing the concrete permeability by lowering the water binder ratio [16, 17]. The aim of this study is to improve the sustainability of water treatment reservoir concrete subjected to $Al_2(SO_4)_3$ in order to extend the life of these reservoirs. This investigation was carried out by EIS. To this purpose, we replaced the cement of the concrete of reservoirs, which is considered a control (containing 100% OPC), by FA at two percentages of 15% and 25%. As concrete needs a long time to be attacked by corrosion, researchers are using laboratory techniques to accelerate the attack. The applied tension technique is an accelerated corrosion testing technique, which indirectly provides information on the characteristics of concrete. So, acceleration of sulphate attack was performed by imposing a potential (15 V). Finally, XRD was carried out on the concrete specimens removed near the surface to examine the corrosion products.

Material and Methods

Materials

The composition of the concrete mixtures used for the preparation of specimens is presented in table 1. The chemical compositions of both the cement and the FA are summarized in table 2. In addition, the size distribution plots for the cement and FA are presented in figure 1. It is determined using laser particle size analysis (Lafarge-Morocco). Scanning electron microscope image of FA and the diameter of the samples are displayed in figure 2 and figure 3, respectively. FA are nanoscale materials. The coarse and fine aggregates, cement, and FA were first mixed in the 210 L drum mixer for approximately 2 minutes. Water was then added to the mix, and all the materials were mixed until a homogeneous mixture was obtained. Then, the fresh concrete was placed into PVC molds and consolidated by means of a vibrating table. After 24 hours, the samples are removed from the molds. The samples were then cured under conditions (23 ± 1 °C and 100% relative humidity) for a period of 28 days. They were then immersed in the 3.5% $Al_2(SO_4)_3$ solution to begin the study.

Corrosion accelerated testing

The durability of three types of concrete exposed to 3.5% $Al_2(SO_4)_3$ was evaluated. This concentration was chosen as the high experimental concentration for the accelerated laboratory tests, which exists in the concentration range from 3000 to 6000 mg/L SO_4^{2-}, which corresponds to exposure class XA3 (Aggressive chemical environments), according to standard

Table 1: Mixtures of concrete (kg/m³).

Concrete mixtures	F1 (0%FA)	F2 (15%FA)	F3 (25%FA)
OPC kg/m³	400	340	300
Sand 0/1 mm kg/m³	580	580	580
Fine aggregate 03/8 mm kg/m³	400	400	400
Coarse aggregate 18/16 mm kg/m³	760	760	760
Water kg/m³	168	168	168
FA kg/m³	-	60	100
E/C	0.42	0.42	0.42

Table 2: Cement and FA chemical composition given by X-ray fluorescence.

Type of cement	OPC	FA
Al_2O_3	3.683	33.4
CaO	58.42	4.44
CaO_1	-	3.92
Cl	0.01	.
CO_2	-	-
Fe_2O_3	2.361	3.35
FeO	-	-
K_2O	0.56	0.81
MgO	2.55	2.06
Na_2O	0.06	1.13
Na_2O_{eq}	0.455	-
SiO_2	15.18	39.5
SO_3	2.59	0.4
P_2O_5	-	1.91
LOI	14.58	8.54

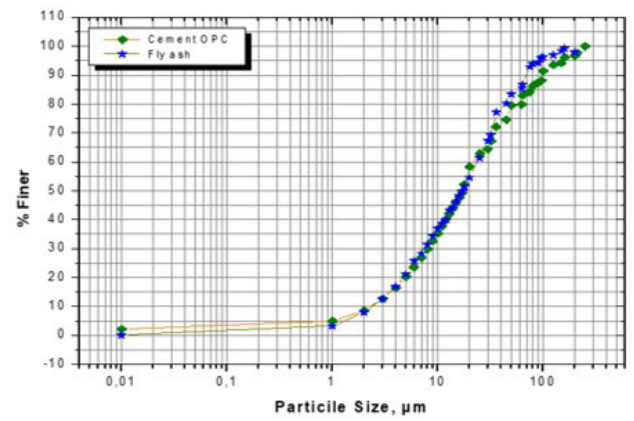


Figure 1: Laser particle size distribution of cement and FA.

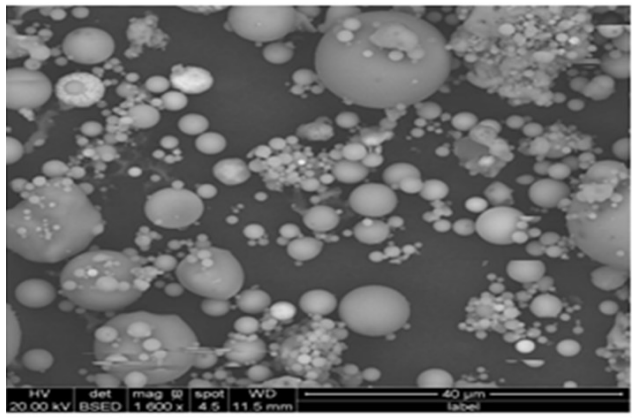


Figure 2: Scanning electron microscope images of FA.

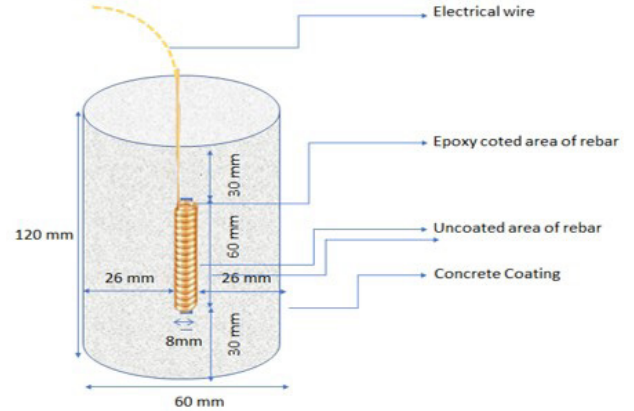


Figure 3: Dimension of the specimen.

NF EN 206-1, while the values used for the treatment of drinking water in reservoirs range from 15 to 100 g/m^3. A DC power supply was employed to apply a 15 V constant potential to the rebars as shown in. Every 24 hours of the accelerated corrosion cycle, the samples were left standing for 48 hours without accelerated corrosion to reach a corrosion steady state. Then, an EIS measurement is performed. Another corrosion cycle (accelerated/rest) is performed after this measurement. All samples were connected in parallel to the DC power supply. They were exposed to the same 15 V voltage to determine the sustainability of concrete. Because the sustainability of concrete depends on its ability to inhibit the penetration of cations and anions [18, 19]. Three electrodes were used to evaluate the electrochemical response: the armature was used as the working electrode, a saturated calomel electrode served as the reference electrode, and a platinum electrode served as the counter electrode. In the present study, all the EIS measurements were performed over the frequency interval from 100 kHz to 10 mHz. The results have been modeled and analyzed using the EC-Lab Analyzer program.

XRD analysis

Sample small quantities of powder identical samples of F1, F2 as well as F3, were prepared for XRD identification in the Bragg-Brentano reflection geometry of the X'Pert3 Powder PANanalytical diffractometer, employing a Cu Kα anode radiation source set at a voltage of 45 KV and a current of 40 mA. The continuous scan range was 5 - 90° 2θ with a step size of 0.02° 2θ.

Results and Discussion

Compressive strength

Compressive strength test values at 7 and 28 days were measured according to Moroccan standards NM10.1.005. The results are presented in figure 4.

The findings indicate enhanced compressive strength of F1, F2, and F3 with increasing curing time. These results are attributed to the continuous hydration reaction of the non-hydrated cement constituents to generate C-S-H that fills the pores [8-20]. In addition, the compressive strength of F2 and F3 is higher than F1. This improvement is attributed to pozzolanic reactions [21] caused by FA that produces additional C-S-H responsible for a denser and more compact microstructure [22, 23]. Furthermore, the surface roughness of the FA particles and their small size, as well as the irregular size of the FA particles (Figure 2), allowed a better interlocking with the cement paste, which leads to a better interfacial transition zone between aggregates as well as the matrix paste [24].

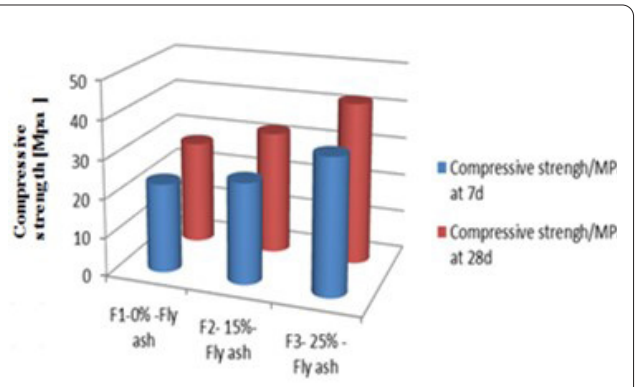


Figure 4: Evolution of the compressive strength of concrete F1, F2, and F3 at 7 and 28 days.

EIS analysis

Figure 5a, 5b, and 5c illustrate the Nyquist graphs of concretes F1, F2, and F3 subjected to a 3.5% $Al_2(SO_4)_3$ solution. The figures reveal an increase in the diameter of the semicircle at low frequency. Furthermore, the graphs shift to

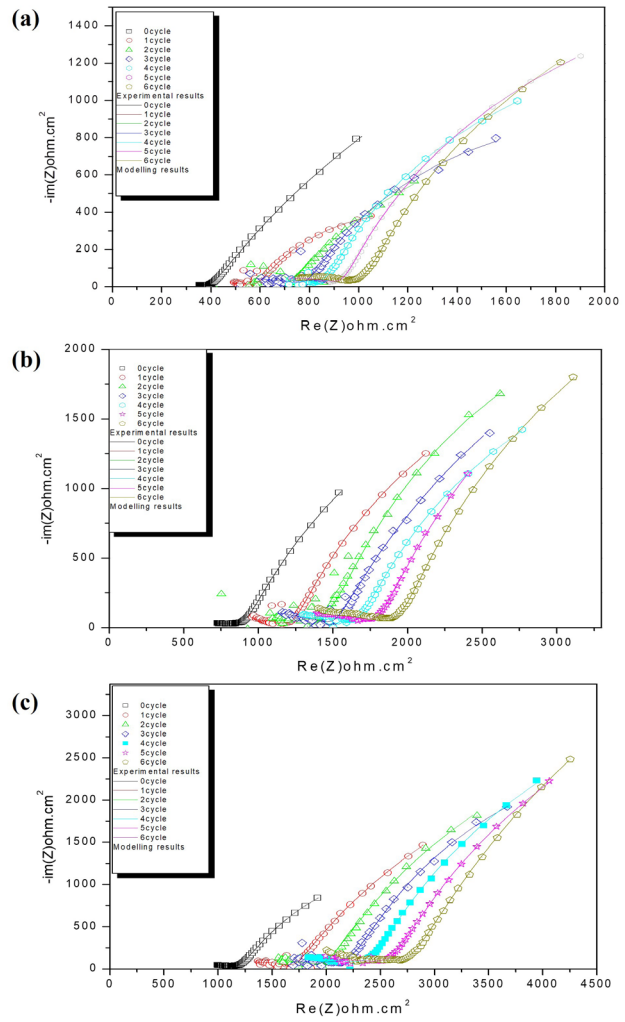


Figure 5: Nyquist diagrams for concrete: **(a)** F1, **(b)** F2, and **(c)** F3.

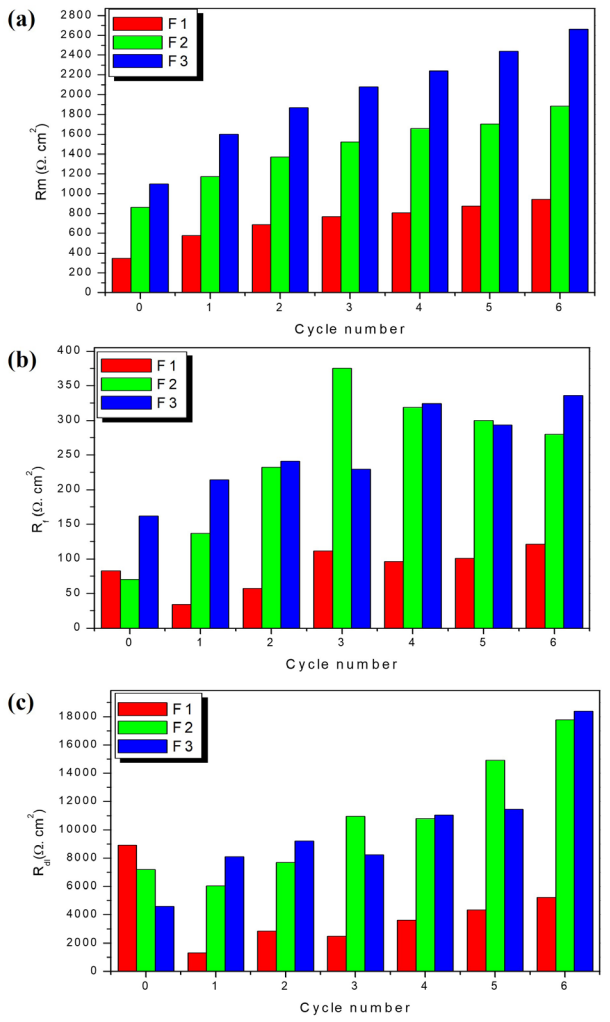


Figure 7: Evolution of resistances **(a)** R_m, **(b)** R_f, and **(c)** R_{dl} of concretes F1, F2, and F2 after the end of the test.

the right indicating the reduction of electron transfer between the steel surface and the corrosive medium and the increase in durability of the concrete coating [25]. For the interpretation of these experimental results, an equivalent electrical circuit (Figure 6) was employed to model the impedance diagrams [26]. Table 3 shows the electrochemical parameters obtained. R_{mortar} is assigned to the bulk resistance properties of concrete coating R_f and CPE_f are respectively referred to as the passive layer resistance and the Constant Phase Element. The charge transfer resistance and the properties of the double layer are represented by R_{dl} and CPE_{dl}. The impedance constant phase element (Z_{CPE}) can be described as:

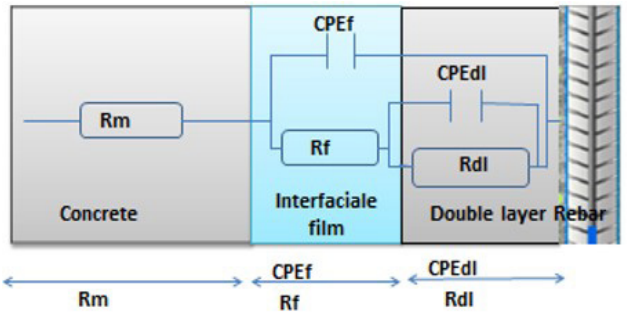


Figure 6: Equivalent circuit used to interpret EIS.

$$Z_{CPE} = \left[CPE(j\omega)^n \right]^{-1} \quad (6)$$

R_{mortar} increases as the accelerated corrosion cycles increase for F1, F2, and F3 (Figure 7a), representing an enhancement of the cementitious matrix properties throughout a test. This behavior is attributed to the reactions of hydration leading to a tendency to fill the voids, allowing the development of the least porous cement matrix during the aging phase, which eventually isolates and protects the reinforcement [25]. Moreover, the resistance of the concretes F3 and F2 increased most obviously, followed by F1. This is due to the pozzolanic behaviour of FA in the cement hydration process, where the SiO_2 and Al_2O_3 compounds in FA interact with $Ca(OH)_2$ [27] to produce C-S-H and C-A-H, resulting in a denser and more concrete coating matrix resistance. In the intermediate frequency, the resistance of the passive film (Figure 7b), (R_f) increases inversely with the non-ideal capacitance CPE_f during the aging process. This is mainly due to the development of a passive film around the steel reinforcement or, due to an increase in the properties of adhesion of the rebar through a passive film due to the basic pH values of the concrete [28]. R_{ct} is the charge transfer resistance which is a direct

Table 3: The values obtained from each electrical component of EC for F1, F2, and F3 subjected to 3.5 % $Al_2(SO_4)_3$ under various accelerated corrosion durations.

Concretes	Cycle number	R_{mortar} (Ω.cm²)	R_f (Ω.cm²)	CPE_f x 10^{-3} (Fs^{n-1} cm^{-2})	n_f	R_{dl} (Ω.cm²)	CPE_{dl} x 10^{-3} (Fs^{n-1} cm^{-2})	n_{dl}
F1	0	347	83	0.26	0.58	8894	4.64	0.79
	1	573	34	1.62	0.97	1295	7.48	0.68
	2	686	57	1.11	0.67	2849	6.37	0.68
	3	766	111	1.09	0.72	2476	3.65	0.80
	3	805	96	1.10	0.73	3624	3.83	0.80
	5	873	101	0.99	0.75	4342	4.02	0.81
	6	942	121	0.97	0.75	5228	3.62	0.80
F2	0	861	70	0.91	0.71	7185	5.34	0.70
	1	1170	137	0.84	0.73	6029	3.37	0.76
	2	1371	232	0.80	0.82	7690	2.42	0.75
	3	1524	375	0.78	0.74	10944	1.72	0.82
	3	1659	319	0.77	0.84	10786	1.89	0.77
	5	1700	300	0.18	0.48	14904	0.65	0.71
	6	1884	280	1.24	0.84	17766	0.60	0.77
F3	0	1097	162	0.78	0.57	4583	3.72	0.71
	1	1600	214	0.66	0.65	8104	2.58	0.71
	2	1868	241	0.52	0.68	9199	2.51	0.75
	3	2080	229	0.70	0.78	8237	2.29	0.75
	3	2240	324	0.77	0.69	11038	1.8	0.78
	5	2437	293	0.69	0.77	11460	2.13	0.76
	6	2660	336	0.90	0.85	18386	1.95	0.75

indicator of the ability of the electrons to transport from the steel into the surrounding matrix/solution [18]. In addition, the charge transfer resistance has the same variation trend (Figure 7c), as the resistance of the concrete coating (R_{mortar}). It can be seen that there was a significant improvement in R_{ct} for F1, F2, and F3 specimens after only 1 cycle of accelerated corrosion probably due to the passivation of steel. On the other hand, the resistance of F2 and F3 is considerably higher than F1 at any given time of corrosion. This could be due to the inclusion of FA, making it difficult for the charge to pass from the surface of the steel to the external medium through the concrete coating.

XRD analysis

Figure 8 displays the XRD pattern of three concrete powders F1, F2, and F3 after the end of the accelerated corrosion test. The concretes have gypsum, calcite, quartz, and portlandite in their composition regardless of the amount of cement replaced by FA. From the graphs, we can see that the majority of the products formed are gypsum. This is consistent with the literature which reports that when the sulfate concentration reaches a certain value (> 30 g/L), the main product of sulfate attack is gypsum [29]. However, when the rate of replacement of cement by FA increases, concretes contain less gypsum and portlandite.

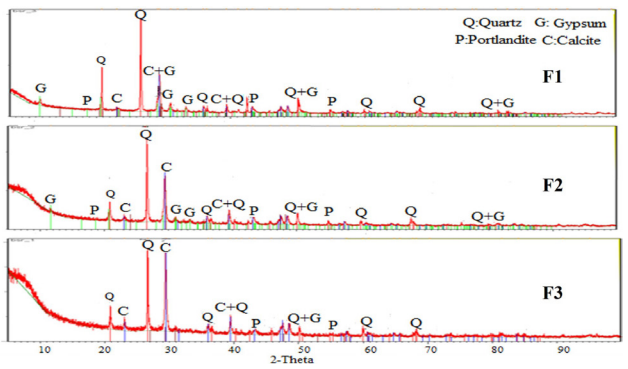


Figure 8: XRD patterns of specimens F1, F2, and F3 after exposed 3.5% $Al_2(SO_4)_3$ solution.

Conclusions

EIS and XRD were used for the present research to assess the sustainability of concrete exposed to 3.5% $Al_2(SO_4)_3$. The conclusions are as follows:

- Compressive strength increases with an increasing percentage of FA.
- The higher R_{mortar} and R_{dl} values of the F2 and F3 concrete relate to the denser, more compact structure as well as the lower conductivity.
- XRD analysis indicated that the gypsum formed in the FA free concrete is high, confirming the beneficial effect of FA against the formation of expansive products in the reservoir concrete.
- The longest durability is that of F3 containing 25% FA.

Acknowledgements

This research study is in the context of the tripartite convention N_ IEA/DDP/2016 ONEE (Office national de l'eau potable-branche eau)-UIT (Université Ibn Tofail)-ENSMR (Ecole nationale de l'industrie minérale de Rabat) Morocco.

Conflict of Interest

None.

References

1. Zouboulis A, Traskas G, Samaras P. 2008. Comparison of efficiency between poly-aluminium chloride and aluminium sulphate coagulants during full-scale experiments in a drinking water treatment plant. *Sep Sci Technol* 43(6): 1507-1519. https://doi.org/10.1080/01496390801940903
2. Demir A, Topçu İB, Kuşan H. 2011. Modeling of some properties of the crushed tile concretes exposed to elevated temperatures. *Constr Build Mater* 25(4): 1883-1889. https://doi.org/10.1016/j.conbuildmat.2010.11.071
3. Ejbouh A, Ech-chebab A, Hassi S, Galai M, Benqlilou H, et al. 2023. Durability assessment of LC^3-based reinforced concrete under combined chloride-sulfate environment via the EIS technique. *Constr Build Mater* 366: 130194. https://doi.org/10.1016/j.conbuildmat.2022.130194
4. Bonakdar A, Mobasher B. 2010. Multi-parameter study of external sulfate attack in blended cement materials. *Constr Build Mater* 24(1): 61-70. https://doi.org/10.1016/j.conbuildmat.2009.08.009
5. Merida A, Kharchi F, Chaid R. 2015. Measure of the chloride permeability of the pozzolana concrete in sulphate middle. *Procedia Soc Behav Sci* 195: 2668-2674. https://doi.org/10.1016/j.sbspro.2015.06.475
6. Neville A. 2004. The confused world of sulfate attack on concrete. *Cem Concr Res* 34(8): 1275-1296. https://doi.org/10.1016/j.cemconres.2004.04.004
7. Galan I, Baldermann A, Kusterle W, Dietzel M, Mittermayr F. 2019. Durability of shotcrete for underground support–review and update. *Constr Build Mater* 202: 465-493. https://doi.org/10.1016/j.conbuildmat.2018.12.151
8. Ech-chebab A, Ejbouh A, Galai M, Hassi S, Berrami K, et al. 2021. Assessing the fly ash effect on the durability of reinforced concrete of water treatment tanks exposed to coagulating ferric chloride by an electrochemical process. *J Bio Tribo Corros* 7: 1-17. https://doi.org/10.1007/s40735-021-00513-8
9. Li Y, Wu B, Wang R. 2022. Critical review and gap analysis on the use of high-volume fly ash as a substitute constituent in concrete. *Constr Build Mater* 341: 127889. https://doi.org/10.1016/j.conbuildmat.2022.127889
10. Tran VM, Nguyen TH. 2022. Enhancing the effectiveness of steam curing for cement paste incorporating fly ash based on long-term compressive strength and reaction degree of fly ash. *Case Studies Constr Mater* 16: e01146. https://doi.org/10.1016/j.cscm.2022.e01146
11. Nanda B, Rout S. 2021. Properties of concrete containing fly ash and bottom ash mixture as fine aggregate. *Int J Sustain Eng* 14(4): 809-819. https://doi.org/10.1080/19397038.2021.1920641
12. Jiang C, Jiang L, Li S, Tang X, Zhang L. 2021. Impact of cation type and fly ash on deterioration process of high belite cement pastes exposed to sulfate attack. *Constr Build Mater* 286: 122961. https://doi.org/10.1016/j.conbuildmat.2021.122961
13. Sumer M. 2012. Compressive strength and sulfate resistance properties of concretes containing Class F and Class C fly ashes. *Constr Build Mater* 34: 531-536. https://doi.org/10.1016/j.conbuildmat.2012.02.023
14. Sharma N, Sharma P, Parashar AK. 2022. An experimental investigation of sustainable concrete by incorporating e-waste and fly ash. *Mater Today Proc* 62: 4188-4193. https://doi.org/10.1016/j.matpr.2022.04.704
15. Huseien GF, Joudah ZH, Khalid NH, Sam AR, Tahir MM, et al. 2021. Durability performance of modified concrete incorporating fly ash and effective microorganism. *Constr Build Mater* 267: 120947. https://doi.org/10.1016/j.conbuildmat.2020.120947
16. Elahi MM, Shearer CR, Reza AN, Saha AK, Khan MN, et al. 2021. Improving the sulfate attack resistance of concrete by using supplementary cementitious materials (SCMs): a review. *Constr Build Mater* 281: 122628. https://doi.org/10.1016/j.conbuildmat.2021.122628
17. Haque MA, Chen B, Javed MF, Jalal FE. 2022. Evaluating the mechanical strength prediction performances of fly ash-based MPC mortar with artificial intelligence approaches. *J Clean Prod* 355: 131815. https://doi.org/10.1016/j.jclepro.2022.131815
18. Chen Z, Zhang G, Yang EH. 2018. Study of steel corrosion in strain-hardening cementitious composites (SHCC) via electrochemical techniques. *Electrochim Acta* 261: 402-411. https://doi.org/10.1016/j.electacta.2017.12.170
19. Ech-chebab A, Ejbouh A, Galai M, Hassi S, Belhaj T, et al. 2022. The individual and combined effect of olive stone biomass ash with coal fly ash on the durability of water treatment tank concrete exposed to ferric chloride. *Chem Africa* 5(6): 2067-2084. https://doi.org/10.1007/s42250-022-00458-6
20. Zhang Z, Wang Q, Chen H, Zhou Y. 2017. Influence of the initial moist curing time on the sulfate attack resistance of concretes with different binders. *Constr Build Mater* 144: 541-551. https://doi.org/10.1016/j.conbuildmat.2017.03.235
21. Amran YM, Soto MG, Alyousef R, El-Zeadani M, Alabduljabbar H, et al. 2020. Performance investigation of high-proportion Saudi-fly-ash-based concrete. *Results Eng* 6: 100118. https://doi.org/10.1016/j.rineng.2020.100118
22. Zhang MH, Malhotra VM. 1995. Characteristics of a thermally activated alumino-silicate pozzolanic material and its use in concrete. *Cem Concr Res* 25(8): 1713-1725. https://doi.org/10.1016/0008-8846(95)00167-0
23. Sun J, Shen X, Tan G, Tanner JE. 2019. Compressive strength and hydration characteristics of high-volume fly ash concrete prepared from fly ash. *J Therm Anal Calorim* 136: 565-580. https://doi.org/10.1007/s10973-018-7578-z
24. Sanchez F, Sobolev K. 2010. Nanotechnology in concrete–a review. *Constr Build Mater* 24(11): 2060-2071. https://doi.org/10.1016/j.conbuildmat.2010.03.014
25. Ejbouh A, Ech-chebab A, Galai M, Hassi S, Benqlilou H, et al. 2022. Calcined clay process for durability performance of concrete pipe in simulated semi-arid area in Morocco. *Mater Today Proc* 58: 1403-1407. https://doi.org/10.1016/j.matpr.2022.02.332
26. Berrami K, Ech-chebab A, Galai M, Ejbouh A, Hassi S, et al. 2021. Evaluation of fly ash effect on the durability of prestressed concrete cylindrical pipe in aggressive soil by electrochemical method. *Chem Data Collect* 32: 100656. https://doi.org/10.1016/j.cdc.2021.100656
27. Ejbouh A, Ech-chebab A, Galai M, Lachhab R, Benqlilou H, et al. 2022. Effects of fly ash and simulation of the natural hot and dry climate of the Moroccan desert region on the durability of prestressed concrete cylinder pipes. *J Pipeline Syst Eng Pract* 13(4): 04022029. https://doi.org/10.1061/(ASCE)PS.1949-1204.0000658
28. Subbiah K, Velu S, Kwon SJ, Lee HS, Rethinam N, et al. 2018. A novel *in-situ* corrosion monitoring electrode for reinforced concrete structures. *Electrochim Acta* 259: 1129-1144. https://doi.org/10.1016/j.electacta.2017.10.088
29. Haufe J, Vollpracht A. 2019. Tensile strength of concrete exposed to sulfate attack. *Cem Concr Res* 116: 81-88. https://doi.org/10.1016/j.cemconres.2018.11.005